THE UNIVERSITY OF MICHIGAN
COLLEGE OF ENGINEERING
Department of Nuclear Engineering
Laboratory for Fluid Flow and Heat Transport Phenomena

Technical Report No. 11

DETERMINATION OF CAVITATION CONDITIONS FROM DENSITY PROFILES OF MERCURY IN A VENTURI

Ian E. B. Lauchlan
Frederick G. Hammitt
Richard D. Ivany
M. John Robinson
Willy Smith

ORA Project 03424

under contract with:

NATIONAL AERONAUTICS AND SPACE ADMINISTRATION
GRANT NO. NsG-39-60
WASHINGTON, D.C.

administered through:

OFFICE OF RESEARCH ADMINISTRATION ANN ARBOR

October 1963

ACKNOWLEDGMENT

The electronic equipment was kindly furnished by the Department of Nuclear Engineering of The University of Michigan.

ABSTRACT

The extent of the cavitation in mercury flowing in a transparent, Plexiglas venturi can be determined by measuring the decrease in the attenuation of a well collimated, Co^{60}, gamma beam in passing through the venturi when voids resulting from cavitation are present. Experimental results for the axial fluid density profile are consistent with the visual appearance of the cavitating flow.

TABLE OF CONTENTS

LIST OF ILLUSTRATIONS

LIST OF ILLUSTRATIONS (Concluded)

I. INTRODUCTION*

The present research investigation on cavitation-erosion damage in flowing systems has utilized transparent (Plexiglas) venturis into which damage specimens have been inserted, both with water and room temperature mercury as the cavitating fluids[2,3]. The use of a transparent venturi has allowed the visual setting of the desired cavitation condition (as delineated by the location of the termination of the cavitation region - see Appendix for definition of various degrees of cavitation). An independent measure of the degree of cavitation has been afforded by the flow and pressure measurements, since the pressure drop across the venturi for a given flow is very sensitive to the extent of the cavitating region. However, it has also been found that the ratio of venturi (stagnation) pressure loss to throat kinetic pressure is a strong function of Reynolds Number and perhaps other variables[4], so that the pressure and flow measurements alone cannot be used, without an independent check, as an indication of degree of cavitation.

As one of the next steps in the cavitation investigation, it is planned to conduct damage tests at somewhat elevated temperatures using mercury, and later molten lead or lead-bismuth alloy, as the cavitating fluids. Since this will probably necessitate a non-transparent (steel) venturi, it becomes necessary to develop a technique for obtaining an independent measurement of cavitation condition other than that derived from pressure and flow measurements,

---

* This report summarizes a previous paper and also presents additional information.

so that the true meaning of these measurements can be ascertained. It is the purpose of this report to describe such a method, and the initial measurements which have been made, using room temperature mercury in a transparent venturi. The technique involves the measurement, by differential gamma-ray absorption, of mean density of the cavitating fluid, in a plane through the centerline, as a function of axial position. It was expected that, with such a density profile, it would be possible to delineate the approximate location of the termination of cavitation, and that this location would agree with that determined visually. As will be shown, this objective has been accomplished, so that effectively the axial density profile can be substituted for the visual indication in the determination of degree of cavitation, at least in those cases where there is substantial cavitation, i.e., not initiation conditions.

New information relative to the form of the cavitating flow has also been obtained from these measurements in conjunction with the radial density contours previously measured[5]. From a combination of these two sets of data, it is possible to compute the void fraction of the central (essentially liquid) portion of the flow, i.e., along the centerline, within the 10% void fraction contours previously[5] obtained, and it is shown that this reaches a peak approximately at the visual cavitation termination point.

II. EQUIPMENT

The gamma-ray densitometer and the general technique have been previously described[5]. For convenience the most significant portions will be summarized here. Figure 1 is a schematic of the loop

used, and Figure 2 is a cross section of the cavitating venturi test section. During the experimental runs, two brass specimens were in place in the metal wear specimen holders.

The electronic equipment and densitometer were of a similar type to that used previously[5]. As before, as required by the dense fluid, an energetic gamma source (Co^{60}) was used. The use of a single channel analyzer permitted the separation of the 1.17 Mev peak from the entire pulse height spectrum, so that only the effect of a single energy photon need be considered in the calculations. Figure 3 is a block diagram of the essentials of the electronic equipment, and Figure 4 is photographs of the set-up.

III. EXPERIMENTAL PROCEDURE

A. Calibration of Electronic Equipment

The electronic equipment was calibrated as previously discussed[5]. To improve stability of the equipment, it was operated for several days before the tests were made, so that it would be completely temperature stable. In addition, the tests were run during the late evening and early morning hours to avoid possible difficulties with power surges on the line.

B. Axial Alignment

The collimator-source assembly was securely mounted on a planing table capable of accurately controlled axial and transverse motion. The planing table was bolted to a welded steel stand which was in turn securely bolted to the loop in the vicinity of the venturi, thereby permitting precise positioning of the collimator-source assembly with respect to the venturi. The location of the center-line

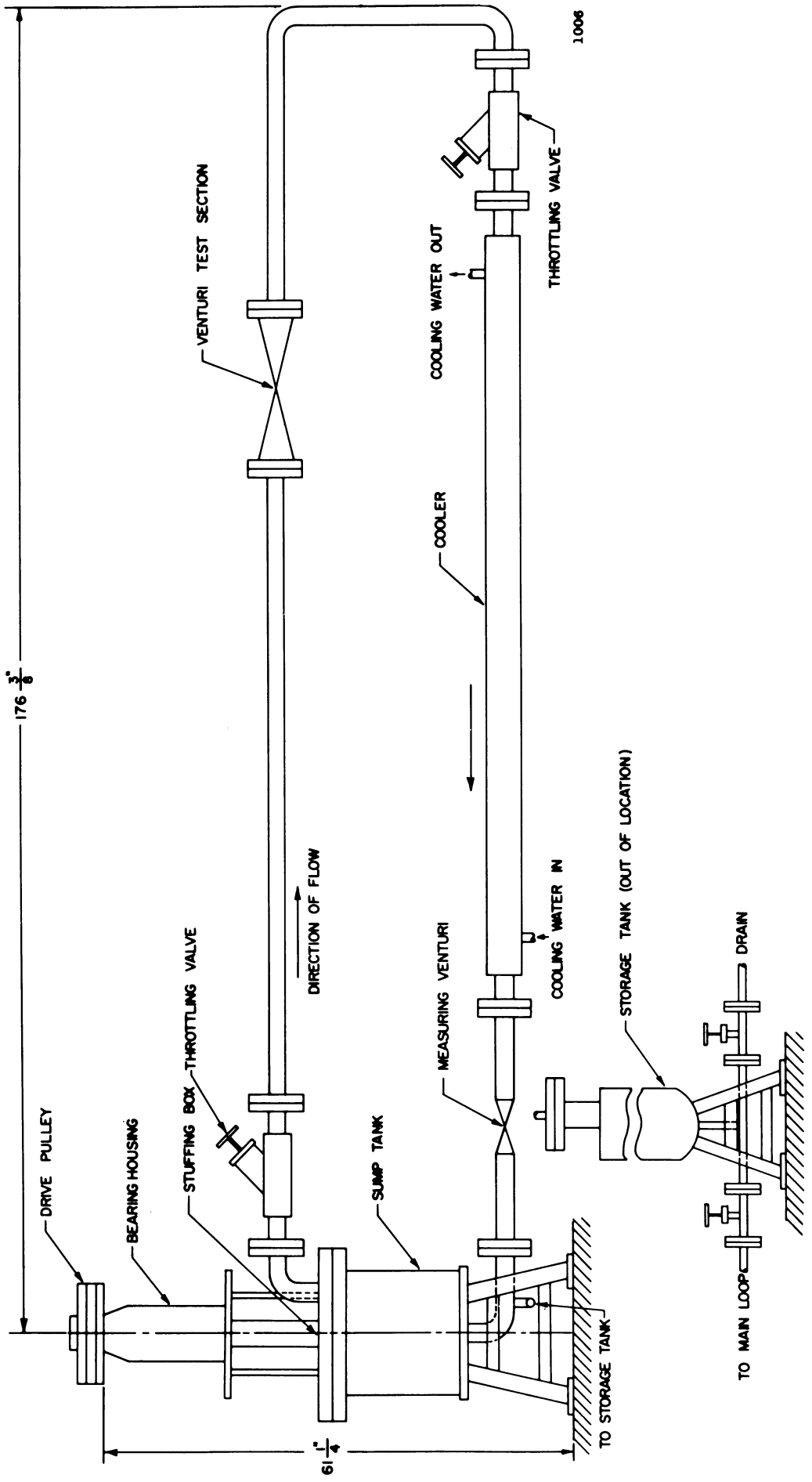

Figure 1. Sketch of overall loop layout.

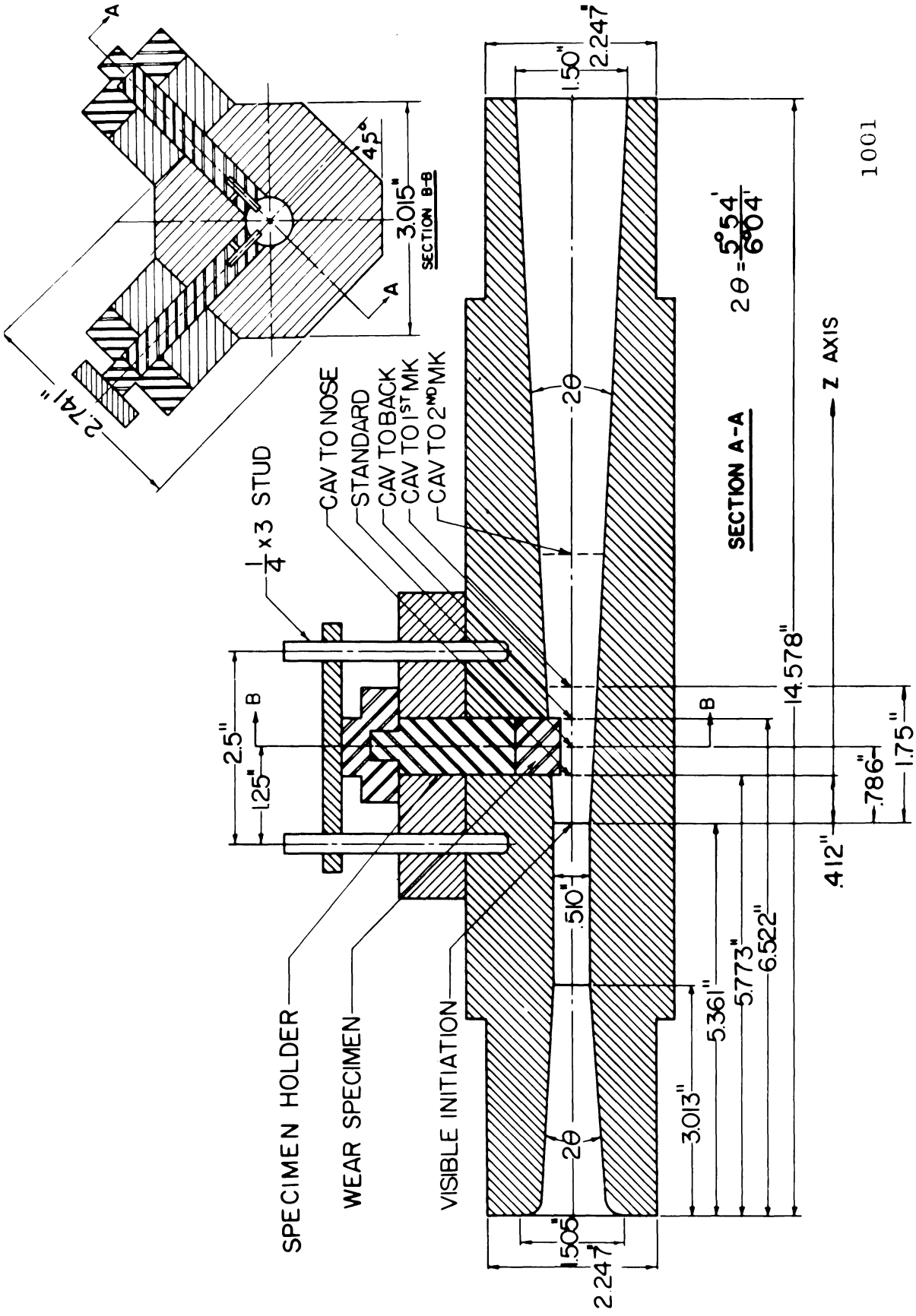

Figure 2. Cross section of cavitating venturi test section showing locations of metal wear specimens and locations of the cavitation termination for various degrees of cavitation.

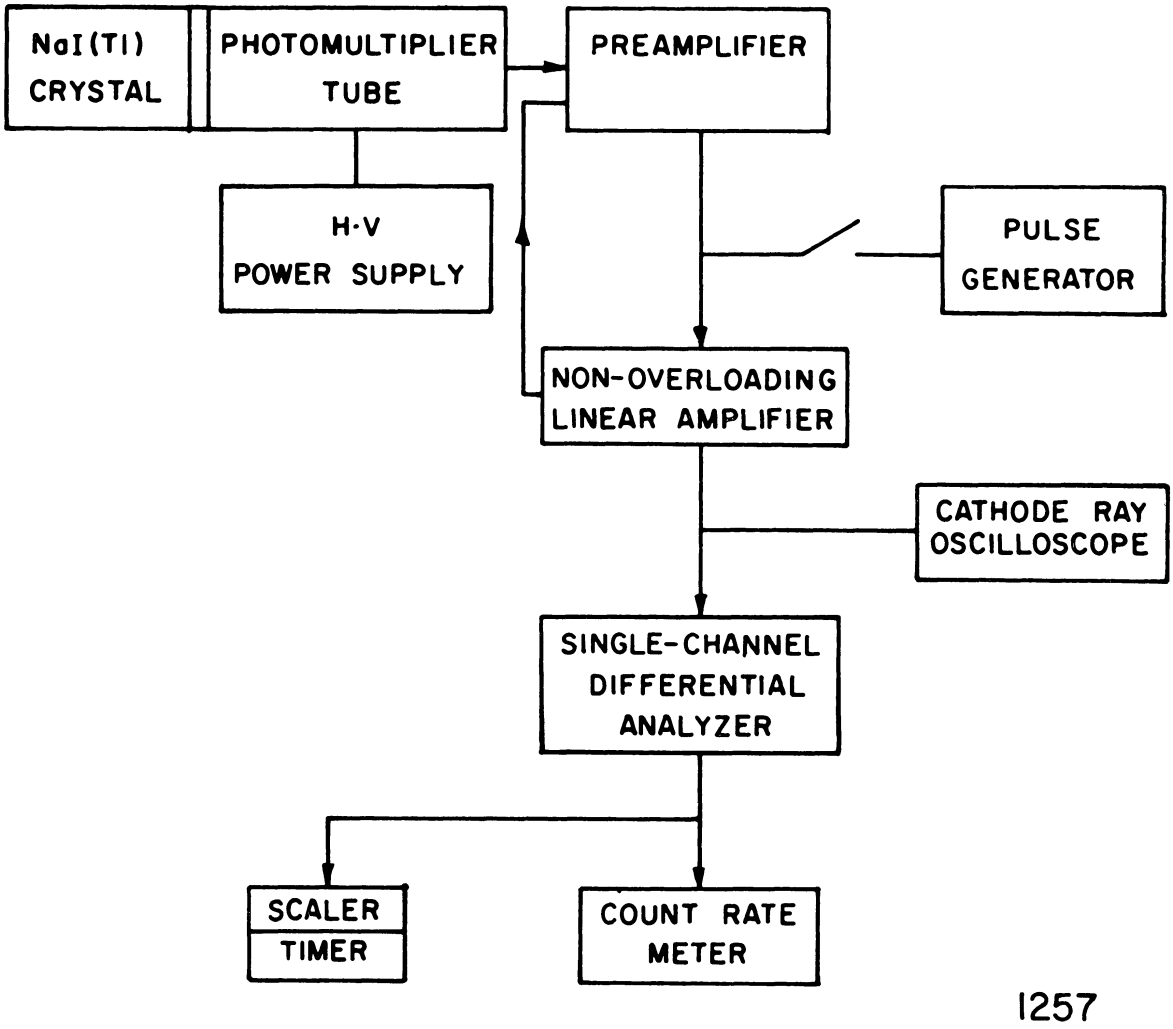

Figure 3. Block diagram of electronic equipment.

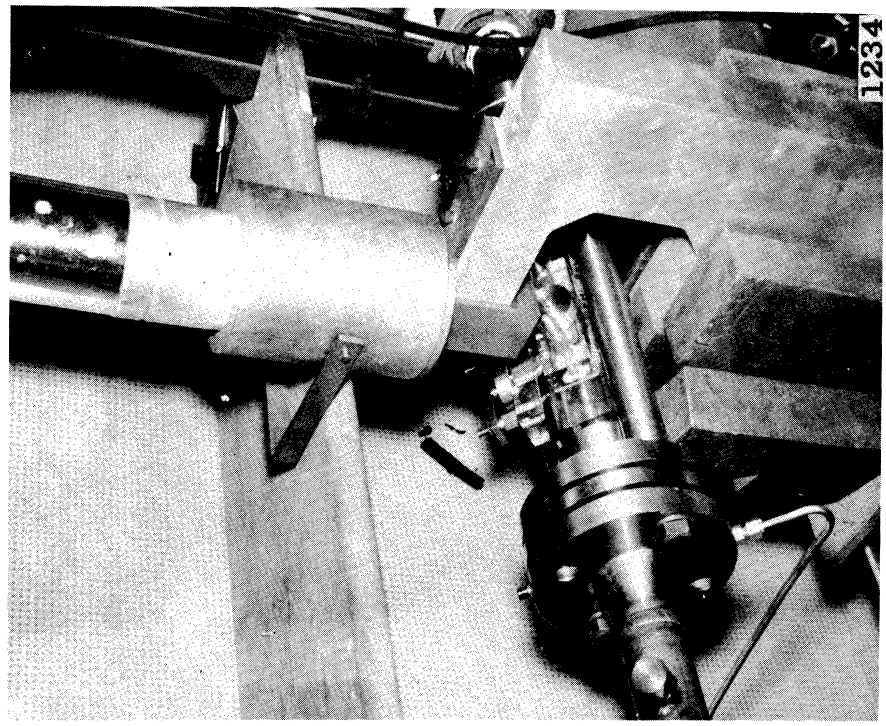

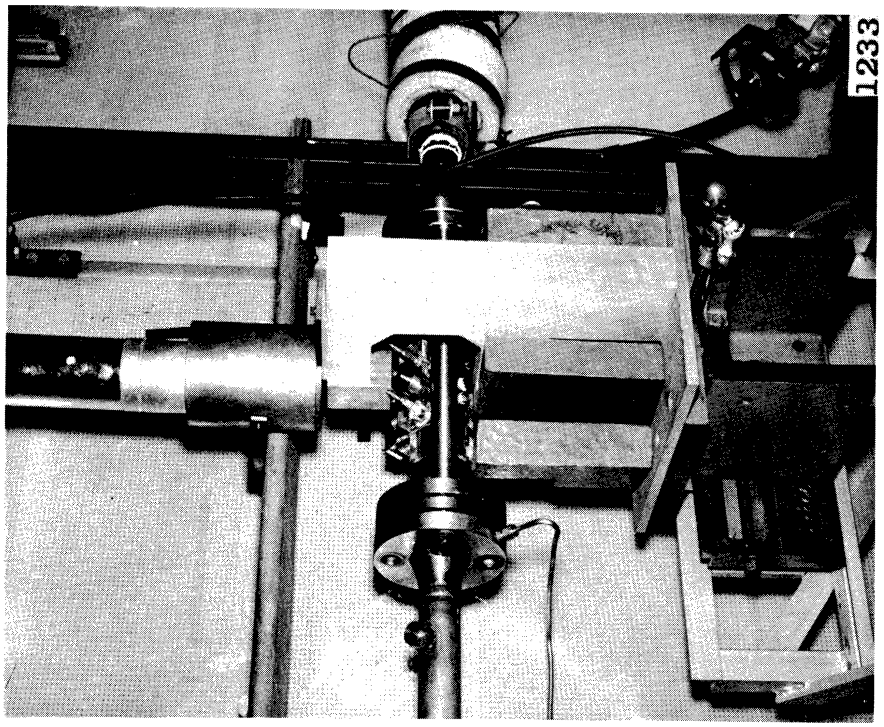

Figure 4. Photographs of densitometer positioned at venturi.

of the venturi relative to the collimator was determined by two independent procedures which were found to agree closely.

i) Optical Alignment Determination

The top and bottom collimator were aligned by placing a light source in the scintillation tube holder, and then moving the bottom collimator so that a maximum intensity would pass through its slit.

The venturi assembly was then placed in position and rotated so that its flat outer surfaces were parallel to the surfaces of the collimators. (This was accomplished by noting that the light would not be refracted when it passed through parallel surfaces). The table was then moved in the transverse (x) direction (Figure 5). The light was refracted in such a manner that it did not enter the slit of the bottom collimator unless it passed through the venturi centerline. In this case the light was not refracted, since all interfaces were normal to the beam (Figure 5). Thus, the centerline of the venturi was established.

ii) Densitometer Centerline Determination Measurement

The Co^{60} source was put in place. The loop was filled with mercury, and a series of count-rate measurements were made at 0.05 inch transverse intervals across the venturi. If axial symmetry is assumed, the centerline presumably coincides with the peak in the count-rate curve (Figure 6).

Since the results of these two independent methods were essentially the same, it is felt that the location of the true centerline of the venturi has been established.

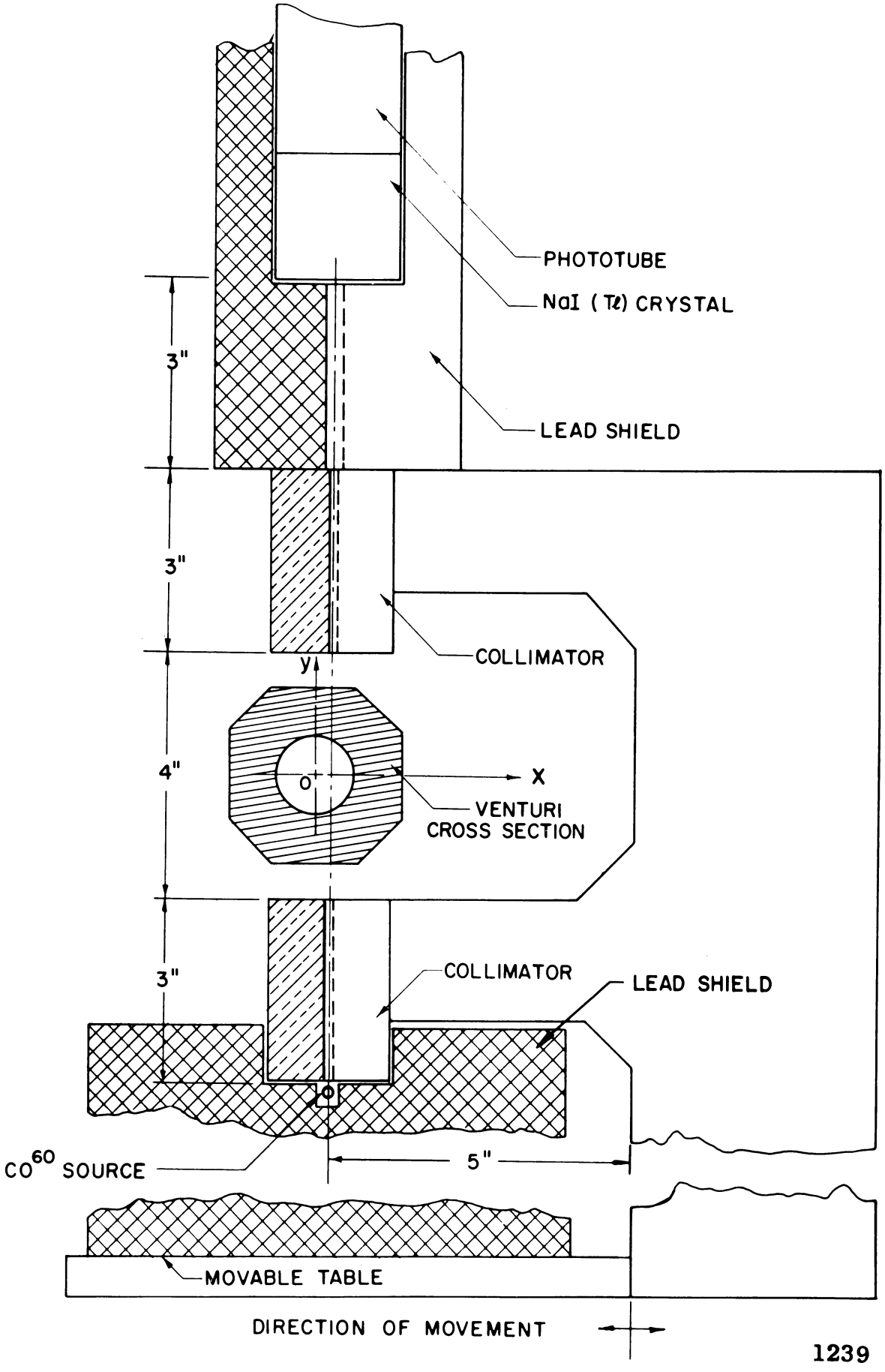

Figure 5. Schematic cross section of densitometer.

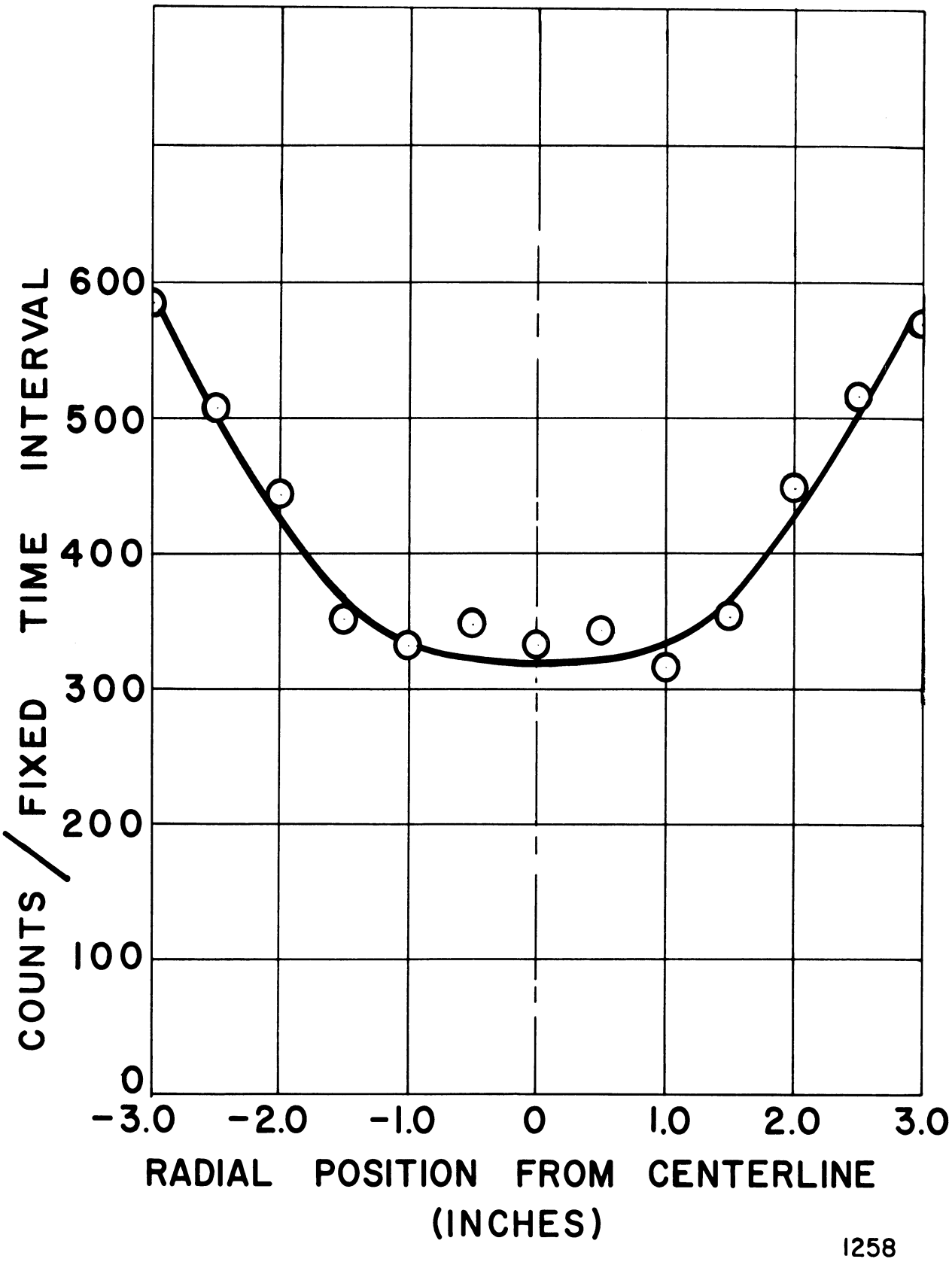

Figure 6. Determination of venturi centerline by densitometer method, assuming axial symmetry.

C. Test Runs

Experimental data were taken by moving the table along the z-axis, parallel to the venturi centerline, and taking readings at z = -0.250, 0.000, 0.250, 0.412, 0.786, 1.163, 1.500 and 1.750 inches. (The throat exit plane of the venturi at the termination of the cylindrical portion, was established as the "zero" for these axial measurements; the positive direction being down-stream). A record was kept of all table motions to insure that the exact table position was known at all times.

Readings were made at all aforementioned positions for both cavitating (see Appendix) and non-cavitating conditions. Background counts were made with and without the pump running to insure that the pump motor was not affecting the detection equipment. Figures 7 through 13 show the experimental count-rates (corrected for background) for the cavitation conditions listed in Table I.

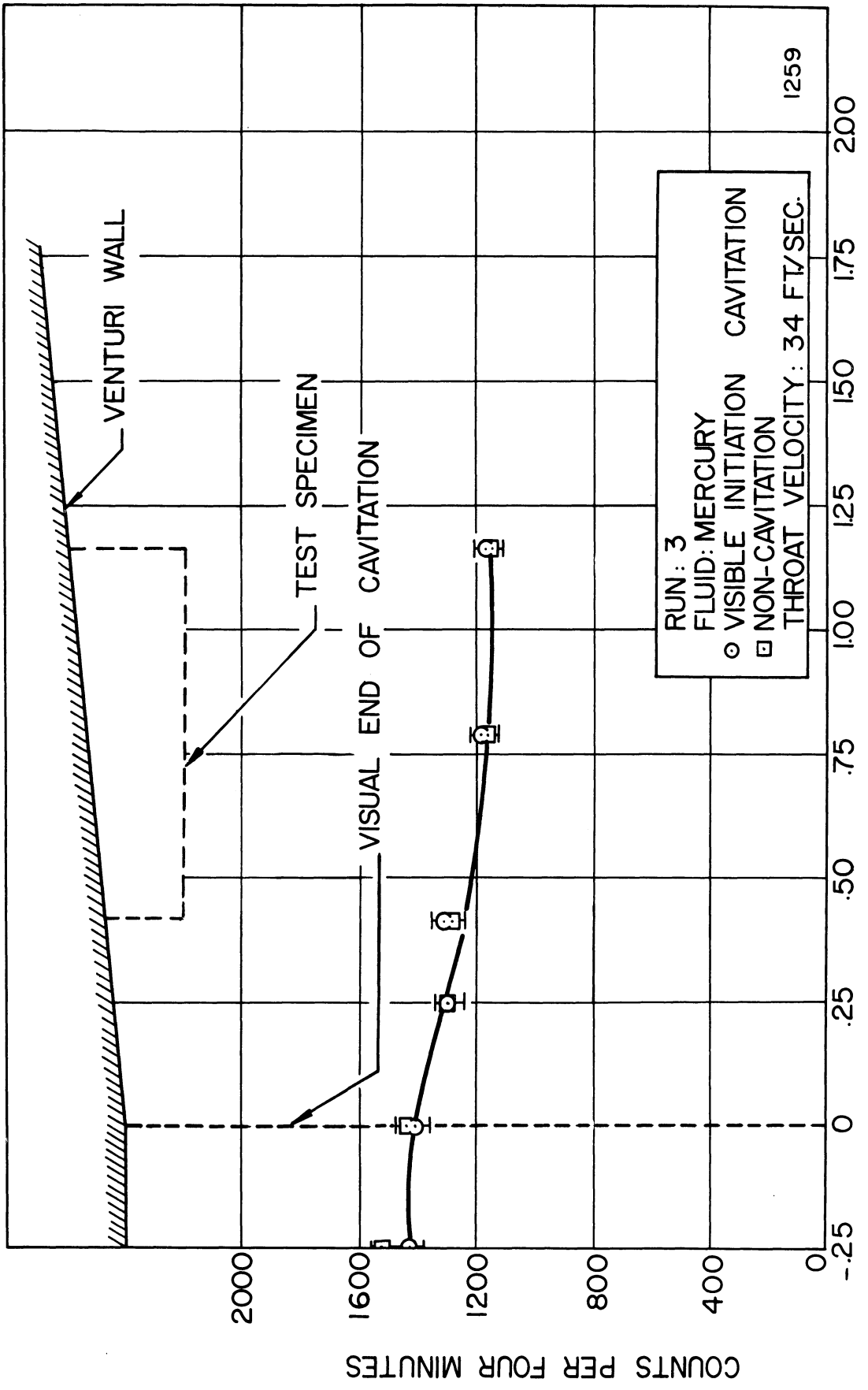

Figure 7. Count-rate vs. axial position for visible initiation at 34 ft./sec. throat velocity.

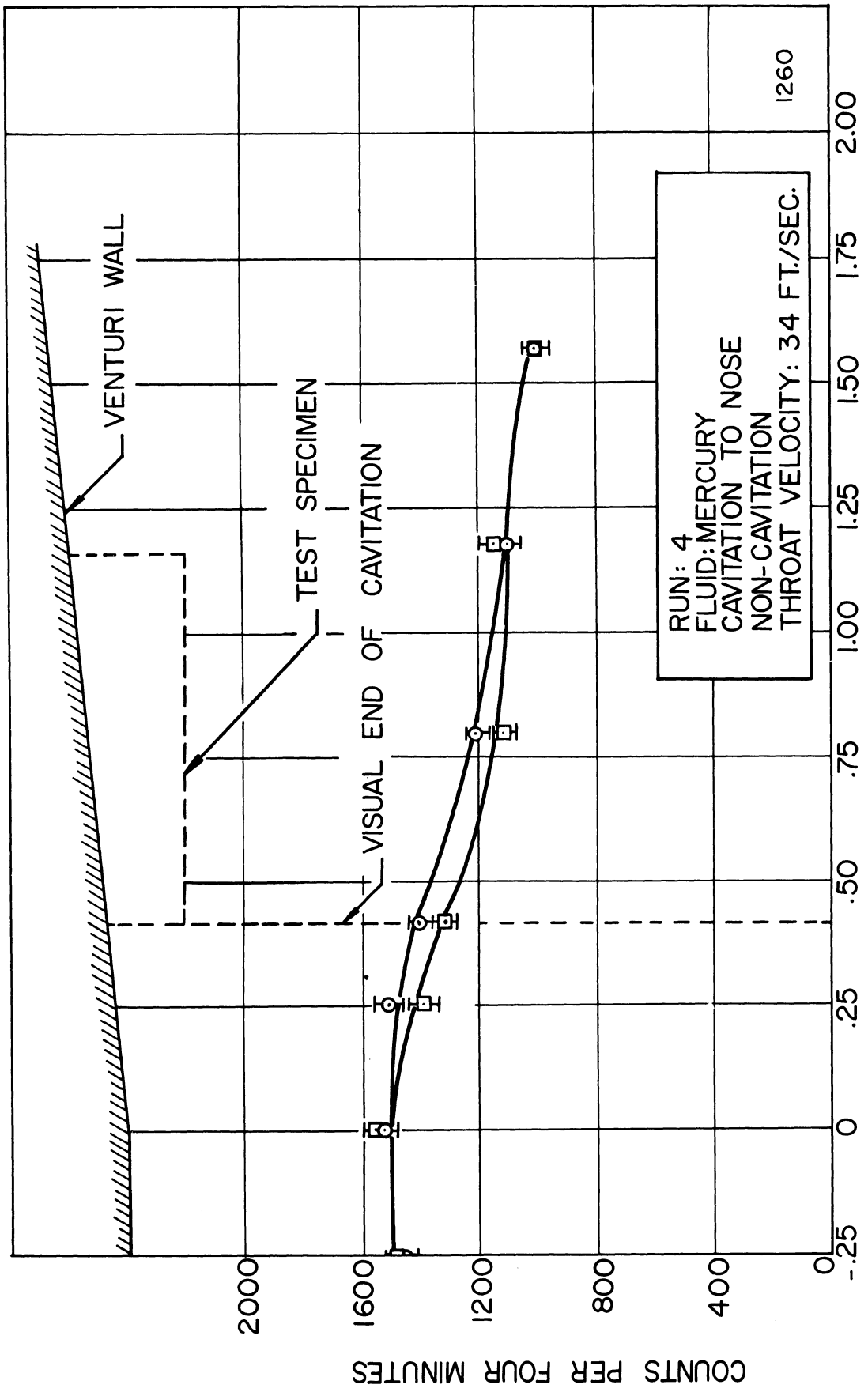

Figure 8. Count-rate vs. axial position for cavitation to nose at 34 ft./sec. throat velocity.

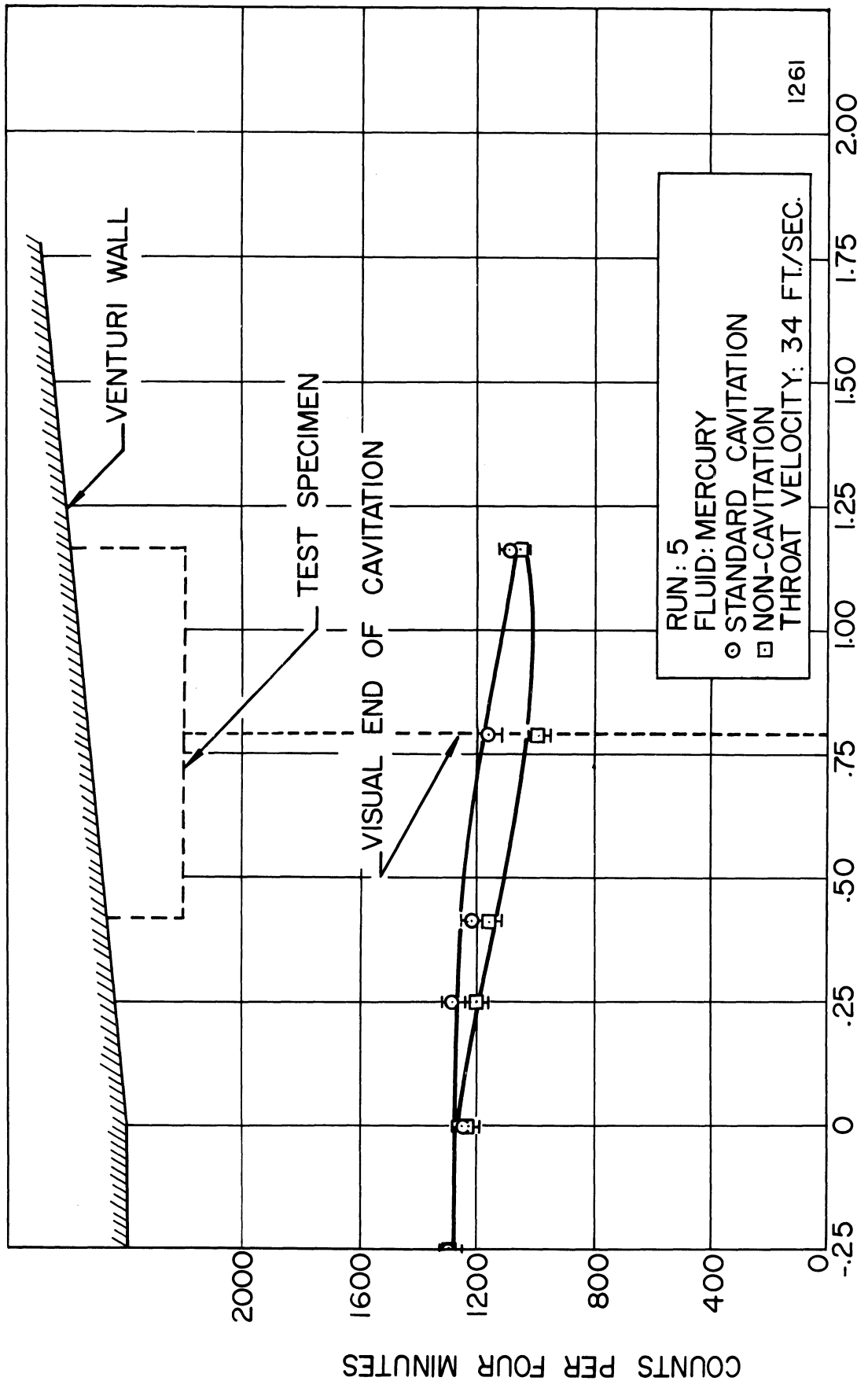

Figure 9. Count-rate vs. axial position for standard cavitation at 34 ft./sec. throat velocity.

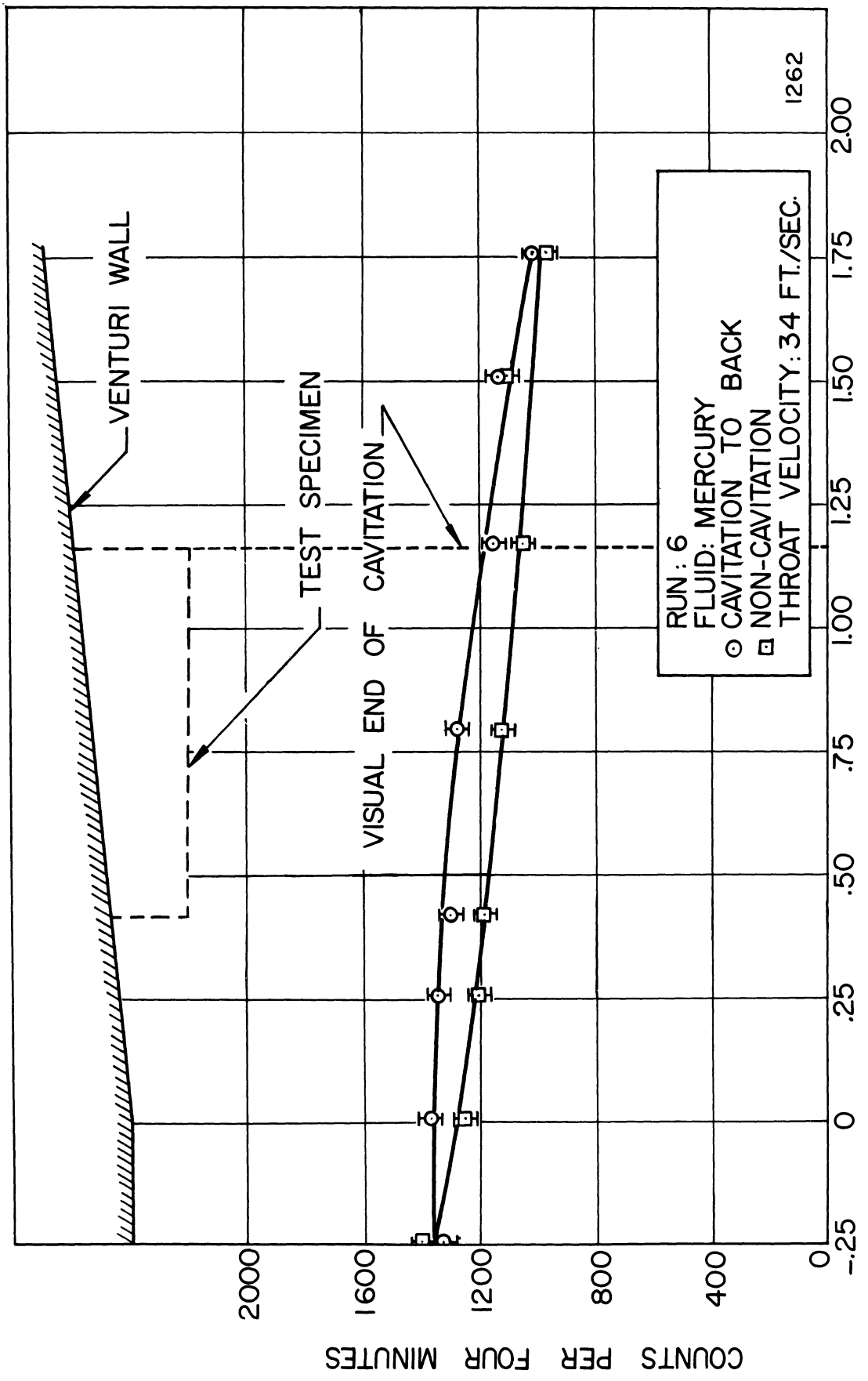

Figure 10. Count-rate vs. axial position for cavitation to back at 34 ft./sec. throat velocity.

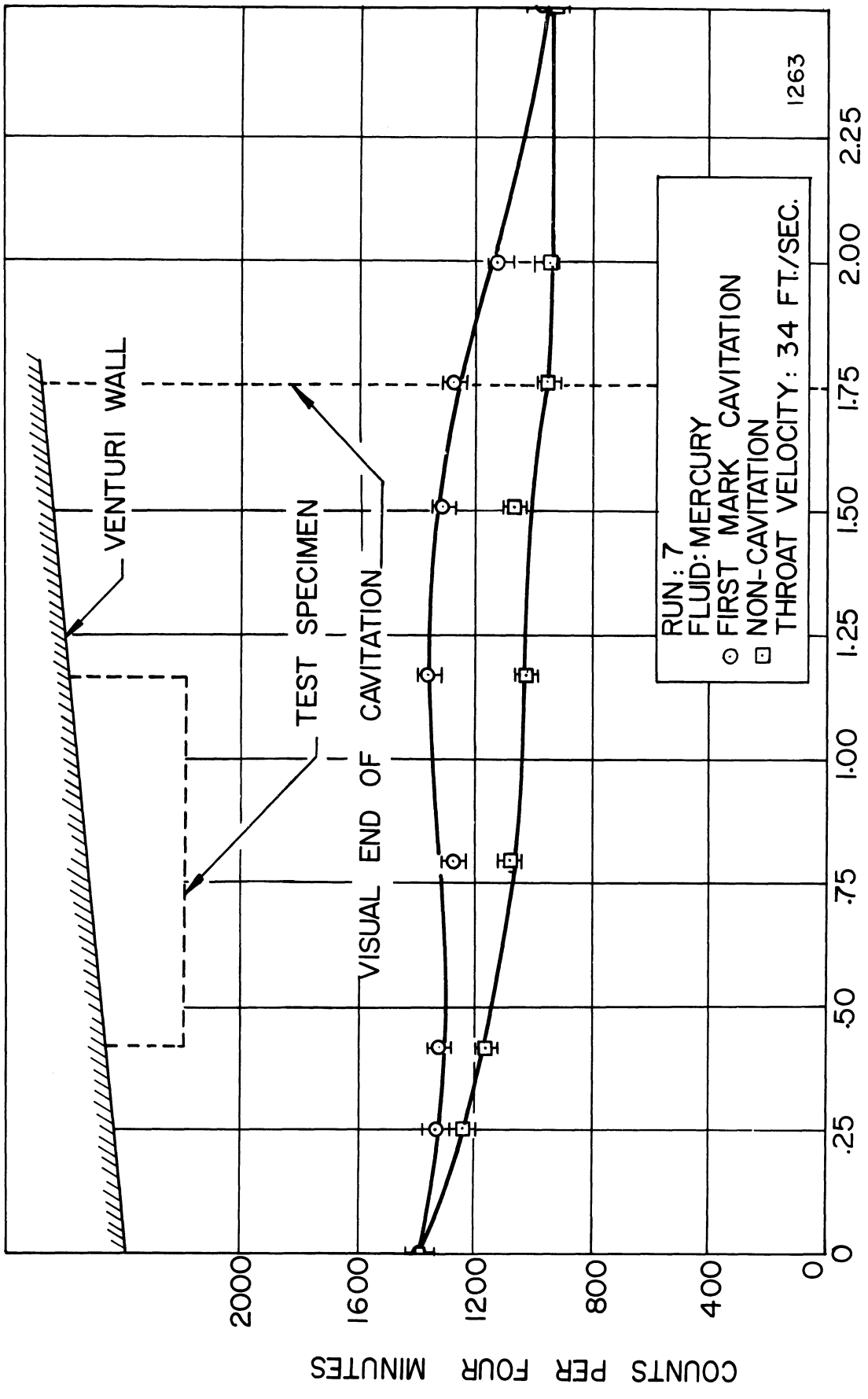

Figure 11. Count-rate vs. axial position for first mark cavitation at 34 ft./sec. throat velocity.

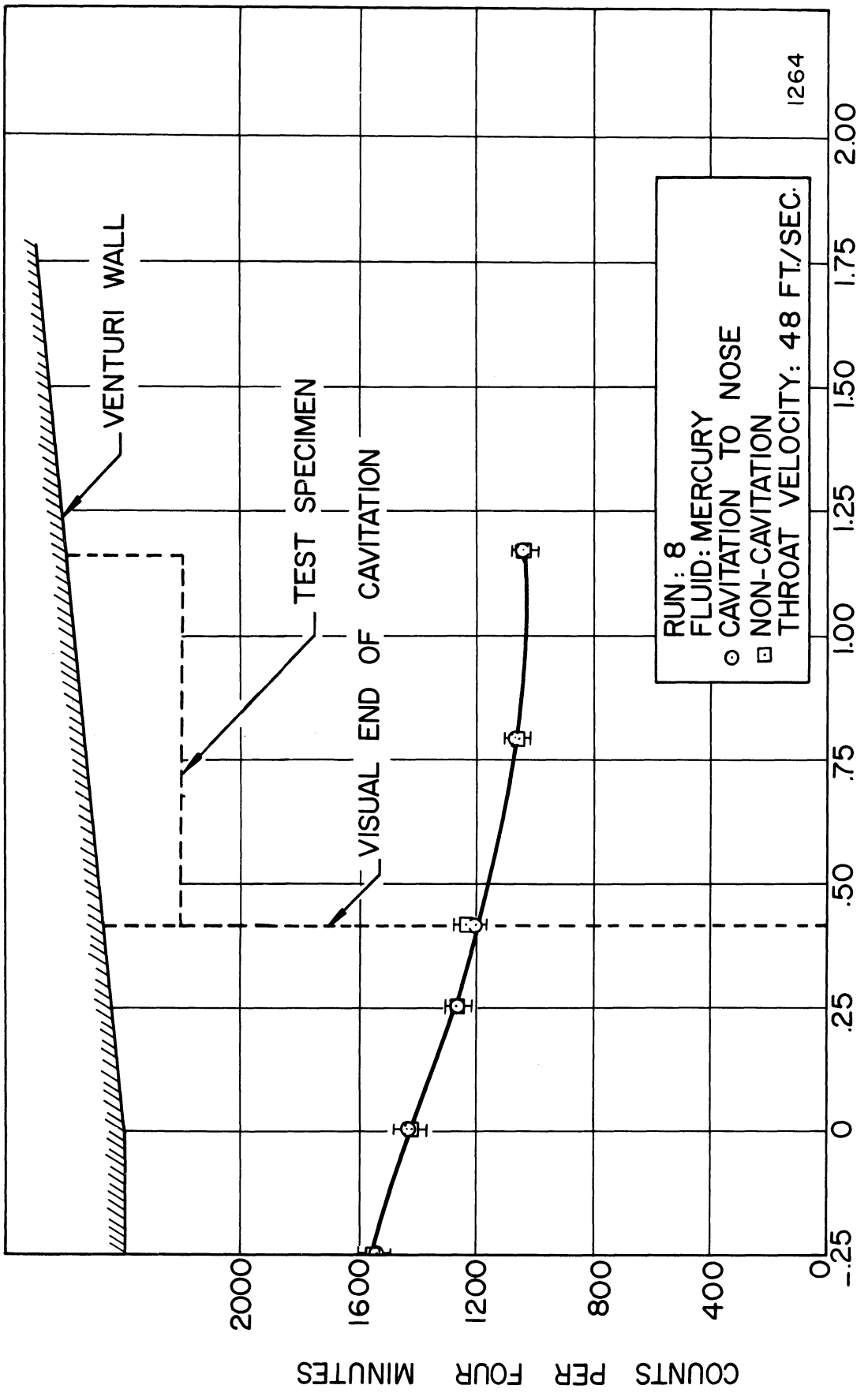

Figure 12. Count-rate vs. axial position for cavitation to nose at 48 ft./sec. throat velocity.

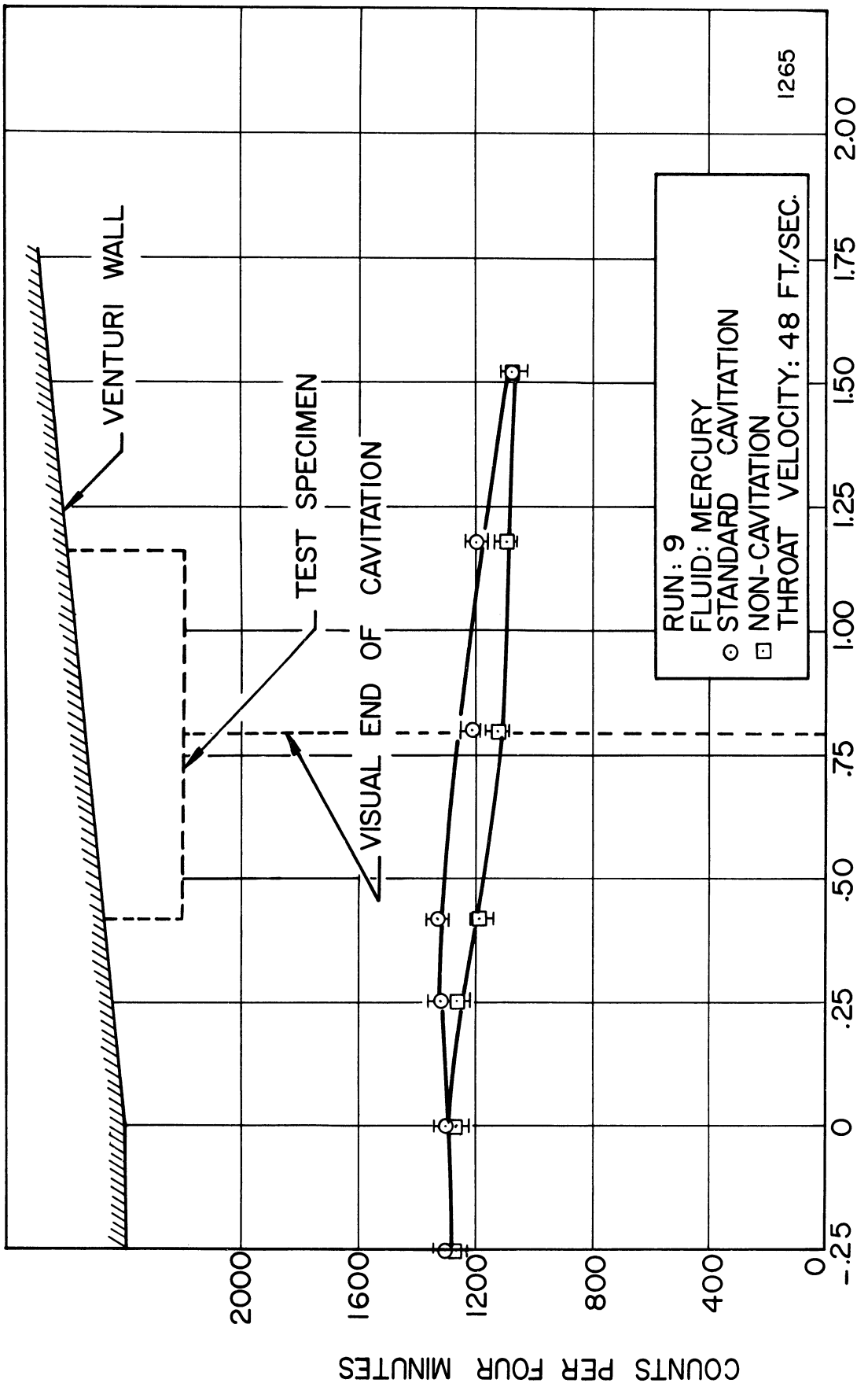

Figure 13. Count-rate vs. axial position for standard cavitation at 48 ft./sec. throat velocity.

TABLE I

Pressure Settings For Mercury Cavitation Conditions

Cav. Condition	Throat Velocity ft./sec.	Venturi Inlet Pressure PSI	Venturi Outlet Pressure PSI	Venturi Pressure Differential PSI
Visible	34	100	73	27
Cavitation to Nose	34	100	69	31
Standard Cavitation	34	100	64	36
Cavitation to Back	34	100	61	39
1st Mark Cavitation	34	100	50	50
Cavitation to Nose	48	225	163	62
Standard Cavitation	48	225	145	80

IV. REDUCTION OF DATA

Figures 7 through 13 show the experimental count rates (corrected for background). Using these experimental points the corresponding density curves were calculated. These are shown in Figures 14 through 20.

Adyanthaya[6] has previously derived a relation between the count rate observed and the density, and this has been repeated in reference 5. That portion which applies to the present case is also summarized in Appendix B.

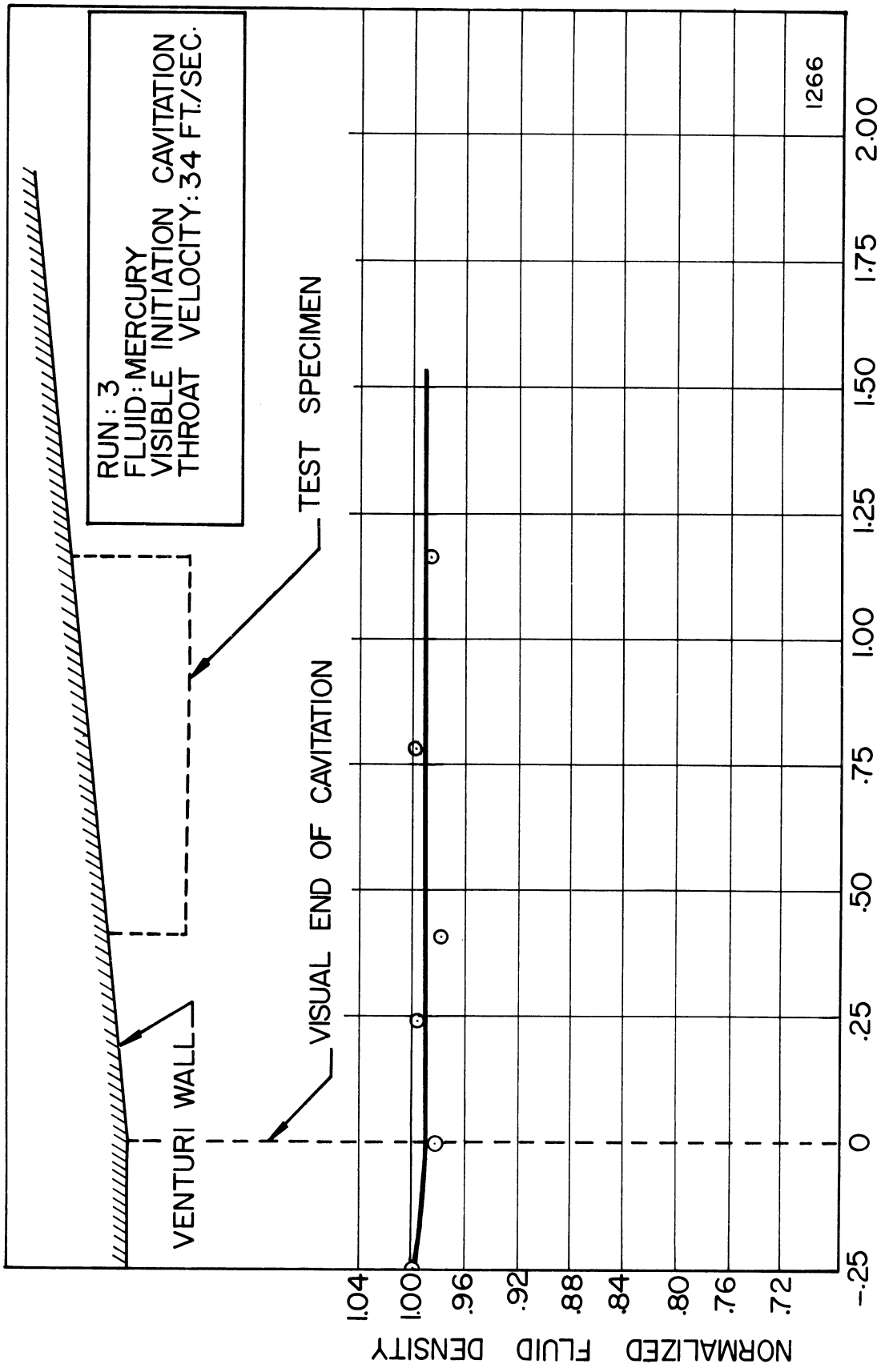

Figure 14. Normalized fluid density vs. axial position for visible initiation at 34 ft./sec. throat velocity.

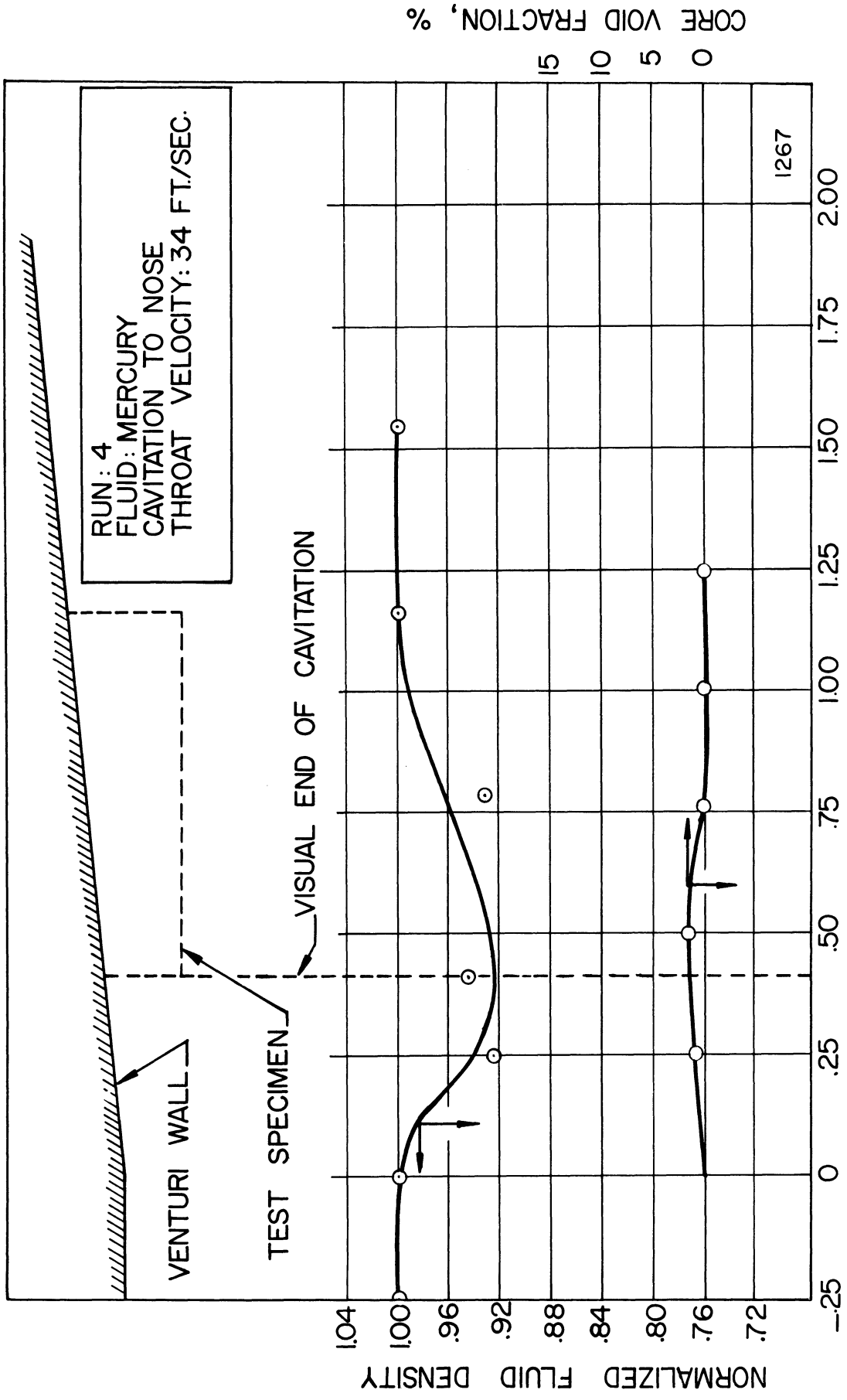

Figure 15. Normalized fluid density and core void fraction vs. axial position for cavitation to nose at 34 ft./sec. throat velocity.

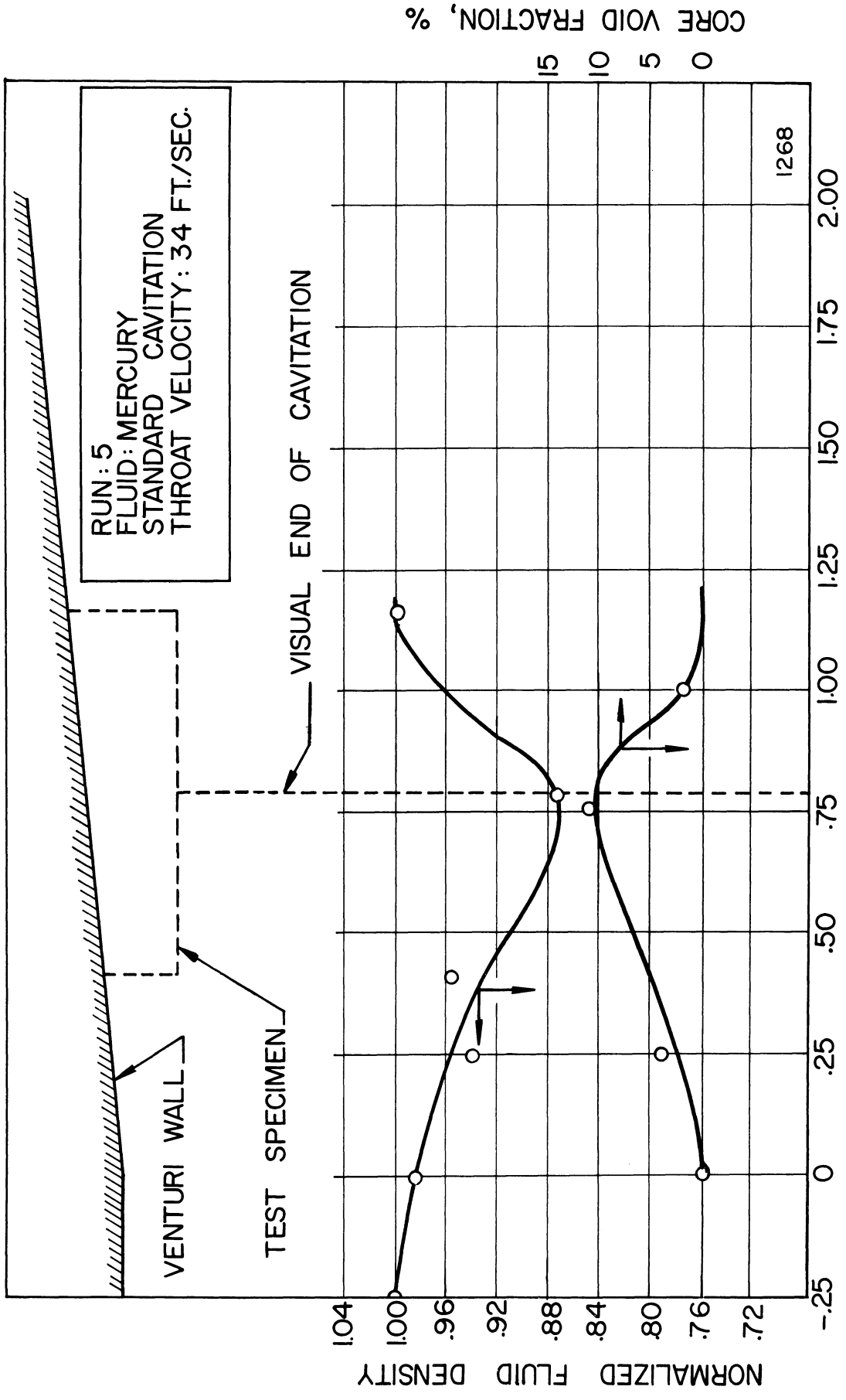

Figure 16. Normalized fluid density and core void fraction vs. axial position for standard cavitation at 34 ft./sec. throat velocity.

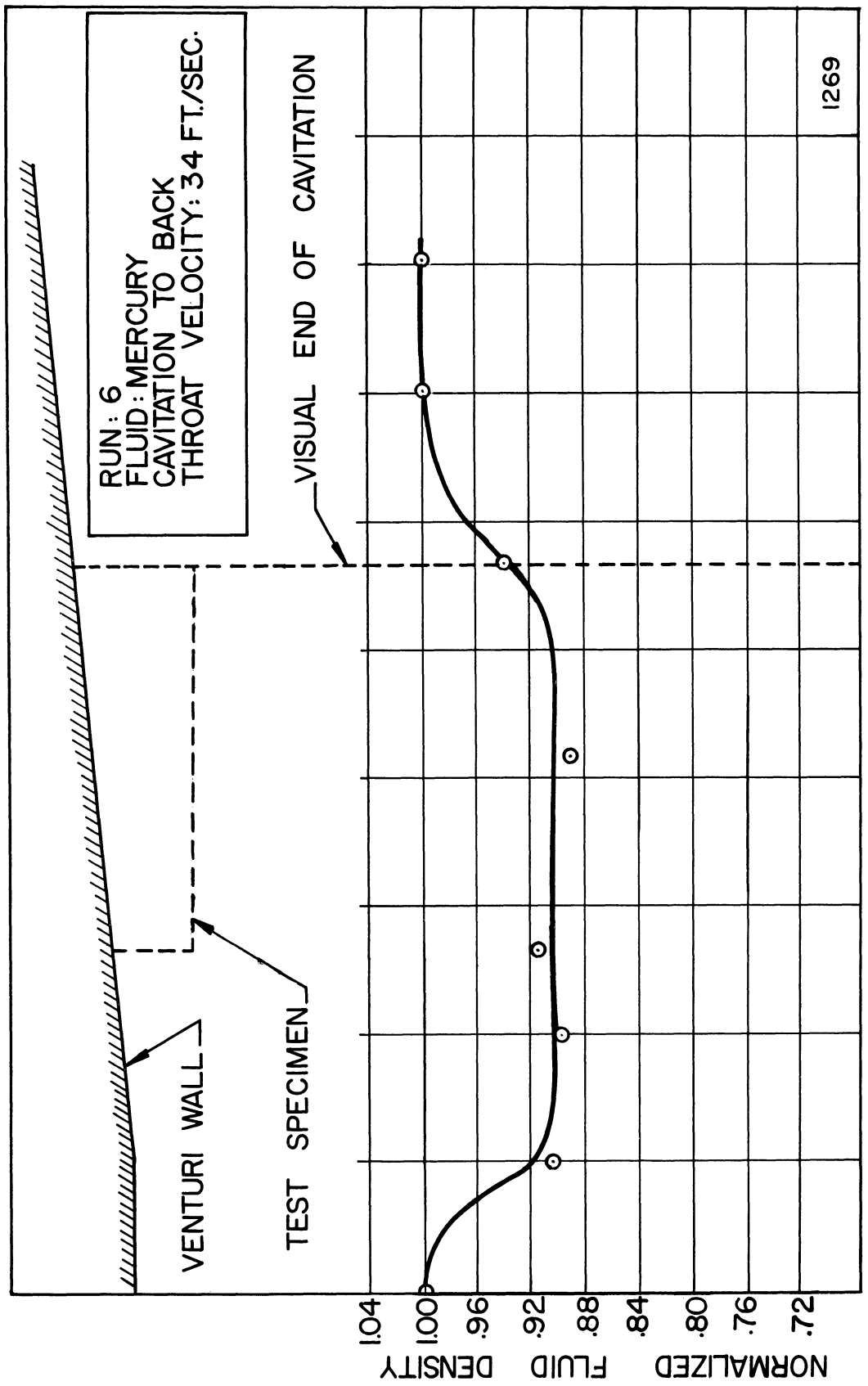

Figure 17. Normalized fluid density vs. axial position for cavitation to back at 34 ft./sec. throat velocity.

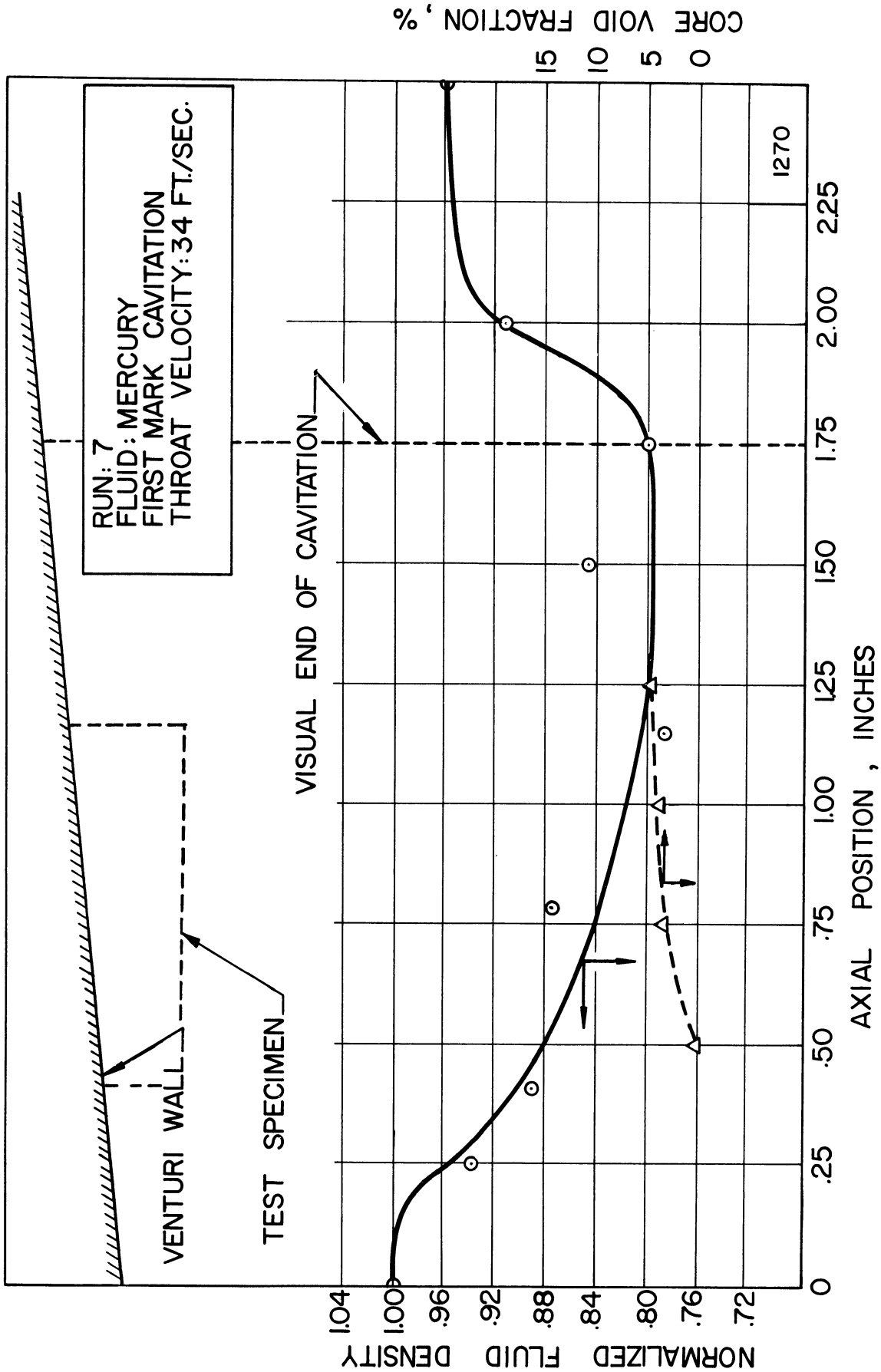

Figure 18. Normalized fluid density and core void fraction vs. axial position for first mark cavitation at 34 ft./sec. throat velocity.

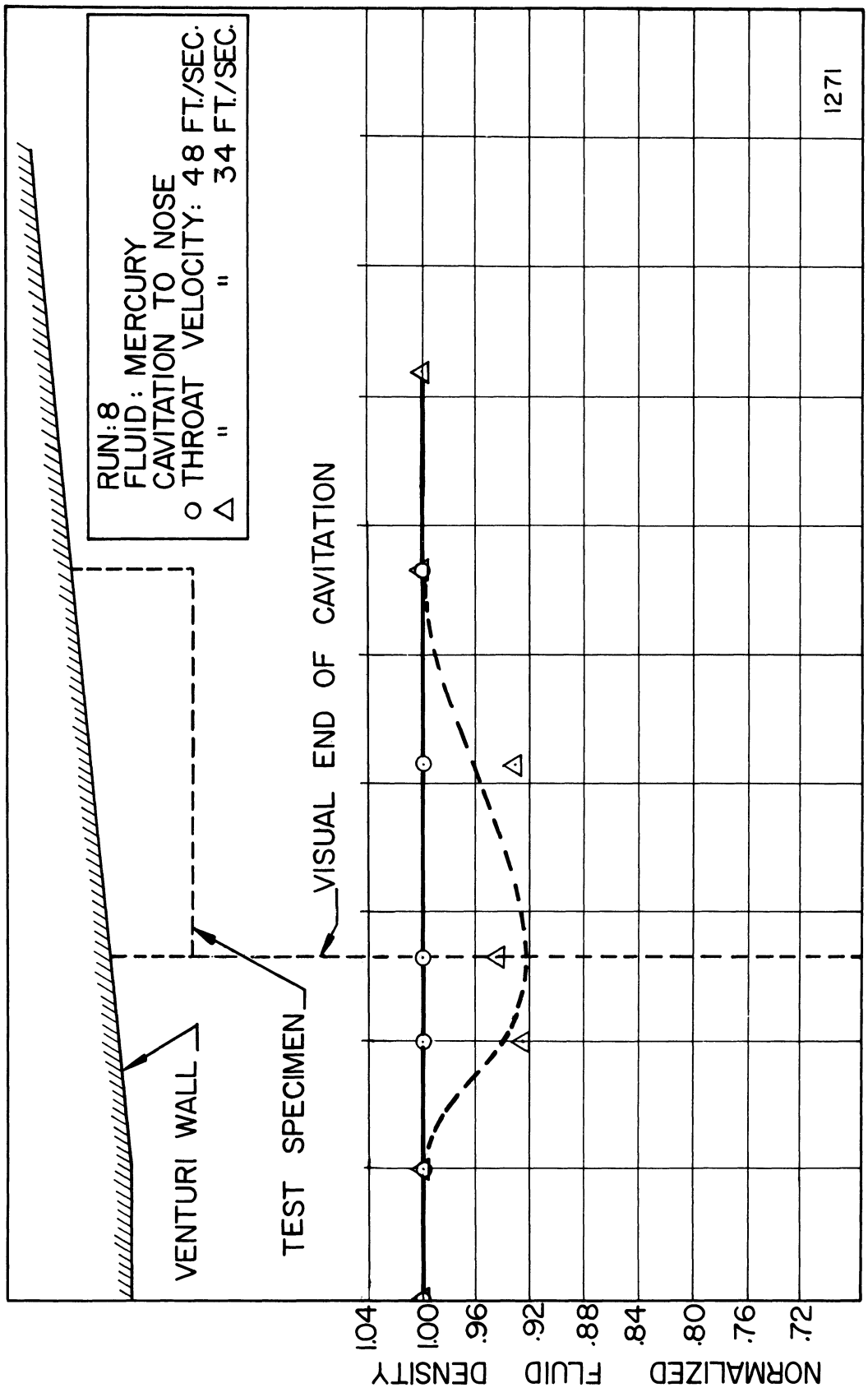

Figure 19. Normalized fluid density vs. axial position for cavitation to nose at 48 and 34 ft./sec. throat velocities.

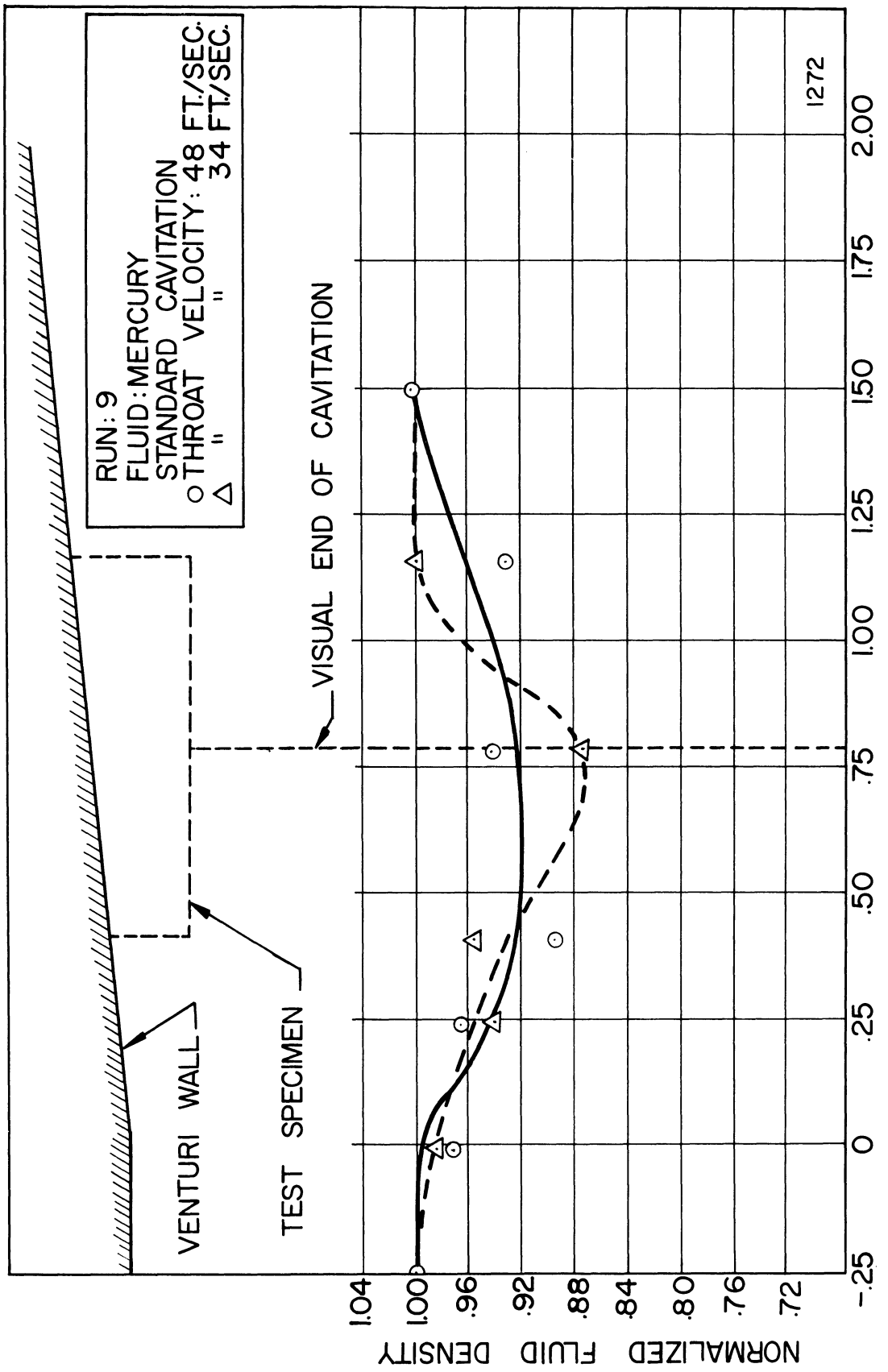

Figure 20. Normalized fluid density vs. axial position for standard cavitation at 48 and 34 ft./sec. throat velocities.

V. DISCUSSION OF RESULTS

A. Axial Density Profiles

An examination of the density profiles (Figures 14 through 20) discloses the following results.

1) Density profiles along the centerline of the venturi are generally sufficient to establish the cavitation conditions other than initiation.* However, this method is not very suitable for determining the visible initiation condition, since the density changes in this mode are not sufficient, considering the statistical fluctuations of counting equipment.

2) Figures 15, 16, 17, 18, and 20 show that the position of the cavitation as determined by the density correlates well with that of the visual settings, corresponding approximately to the start of the rise in the density profile. Since the precision of visual setting was only about $\pm$ 0.10 inches, all the figures cited fall within these limits.

3) Figures 19 and 20 show the effect of throat velocity on the axial density profiles. In both cases, it is noted that the decrease in density in the cavitating region is less for the higher throat velocity, though the visual appearance is the same. No theoretical explanation for this fact is yet apparent. However, a perhaps similar effect has been noted in water tests wherein the transparency of the cavitating region has been greater at higher

---

* The high velocity profile for "Cavitation to Nose", a condition slightly in excess of initiation (Figure 19) shows uniform density. This may indicate a faulty setting of the cavitation condition, or other unknown errors in this particular run.

velocity for the same degree of cavitation.

4) The most consistent results were obtained at the lower throat velocity, perhaps partially due to the greater difficulty of maintaining steady-state during the run duration at the higher velocity, and to the increased mechanical vibrations of the system.

B. Central Jet Axial Density Profiles

As previously mentioned, the axial density profiles already described apply to the mean density of fluid in a vertical plane containing the venturi centerline and extending entirely across the venturi. The density of fluid comprising the central jet in the vicinity of the centerline is also of interest in providing further basic data on the nature of the flow.

By comparison of the present data with those earlier derived[5] from a radial and axial mapping of density profiles in a cavitating venturi of identical dimensions, it is possible to compute the mean density of the central fluid jet within a 10% void fraction contour (minimum measurable void fraction in previous experiment[5]) along the centerline. Such a calculation supplies new basic data, as well as providing a check of consistency between the present data and those of the earlier investigation[5]. The required relations are derived in the Appendix.

The results, in those cases where direct comparisons could be made, are shown in Figures 15, 16, and 18. It is noted that where data are available, the maximum void fraction (minimum density) for the central core approximately coincides with the visual termination point, and hence the minimum density for the entire slice across the venturi. Since the void fraction is generally less than

5% and approaches 10% only in one case (Figure 16), it is apparent that the two investigations are consistent (reference 5 showed this region to possess less than 10% void fraction), and also that the central jet is indeed composed almost entirely of liquid.

C. Experimental Accuracy

Several sources of error inherent in this experiment are:

i) electronics of the system.

ii) measurement technique

iii) assumptions made in the analysis

a) Electronic System Errors

A variation in the gain of the non-overloading amplifier from its calibration would cause a change in the count-rate as would photomultiplier voltage variation. The latter was minimized by using a highly stable high-voltage supply, and by attempting to keep the electronic components at a constant temperature throughout the experiment. A third possible source of electronic error is drifting of the photomultiplier output, as perhaps due to temperature changes, causing a shift in the peak output of the scintillator[7], or by fatigue in the photomultiplier[8]. This third source of error is small since the temperature was kept relatively constant and fatigue effects tend to be high current effects, which is not the present case, i.e., if the anode current can be maintained below 0.1 microamperes, fatigue changes are extremely small at room temperature.

b) Errors in Measuring Technique

Errors in the measurement technique due to positioning of the densitometer were extremely small, since the table could be moved to a specific position with an accuracy of $\pm$ .003 inches. The

main source of error in the measuring technique resulted from the setting of the cavitation condition by a visual method. As mentioned earlier, the accuracy in the visual setting was only $\pm$ 0.10 inches, and it was found difficult to improve the precision significantly by relying wholly upon pressure measurements.

c) Assumptions of Analysis

In the analysis, an "average" density was used. In so doing it is assumed that the voids are small and randomly distributed. It is known, however, that certain non-random distributions, as vertical stratification for example, will give much higher count-rates for the same void fraction. However, it is believed on the basis of Fastax motion pictures that the bubbles are locally random in space-time distribution.

A further assumption, on which both this and the previous investigation[5] were based is that of axial-symmetry. It is believed that on a time-average basis, this is a good assumption though perhaps not at any given instant.

VI. CONCLUSIONS

The cavitation condition for the various degrees other than those approaching initiation may be determined in a non-transparent venturi by making a centerline axial density profile as here described. The position of cavitation termination will approximately correspond to the point where the density profile gradient becomes positive.

The method is not sufficiently sensitive (using the present equipment) to determine initiation. However, a higher count-rate would be desirable in general to reduce statistical fluctuations and

in particular to determine less developed cavitation conditions. Then the count-rate should be within the restriction (0.1 microamperes) presented by photo tube fatigue.

The present data are consistent with those of a previous investigation[5] and a comparison of these two sets of data allows a calculation of the void fraction in the region of the centerline. This is found to become maximum at the approximate axial location of minimum mean density across the venturi.

VII. REFERENCES

1. Lauchlan, I. E. B., "Determination of Cavitation Conditions From Density Profiles", Final Report for Special Project in Course M. E. 600, Mechanical Engineering Department, The University of Michigan, (June, 1963).

2. Hammitt, F. G., "Observations on Cavitation Damage in a Flowing System", Trans ASME, Series D, Journal of Basic Engineering, Vol. 85, (1963), pp. 347-59.

3. Hammitt, F. G., et al., "Cavitation Damage in Mercury and Water in a Cavitating Venturi and Other Components," ORA Report No. 03424-9-T, Nuclear Engineering Department, The University of Michigan, (Sept., 1963).

4. Hammitt, F. G., "Observations of Cavitation Scale and Thermodynamic Effects in Stationary and Rotating Components", Trans. ASME, Series D, Journal of Basic Engineering, Vol. 85, (1963), pp. 1-12.

5 Smith, W., Atkinson, G. L., and Hammitt, F. G., "Void Fraction Measurements in a Cavitating Venturi", ORA Report No. 03424-7-T, Nuclear Engineering Department, The University of Michigan, (Sept., 1962); also as ASME Paper No. 63-AHGT-19, (Mar., 1963), to be published Trans. ASME, Journal of Basic Engineering.

6. Adyanthaya, B. A., "Mercury Void Fraction Measurements Using a Collimated Gamma Ray Beam", Term Paper in Course N. E. 299, Nuclear Engineering Department, The University of Michigan, (June, 1961).

7. Cameron, J. F., et al., "Some Effects of Temperature on the Performance of Scintillation Counters", IAEA Nuclear Electronics, Vol. 1, (1962).

8. Cathey, L., "Fatigue in Photomultipliers", IRE NS-5, 109, (1958).

VIII. APPENDIX

A. Degrees of Cavitation

The cavitation conditions used in this series of measurements and in previous measurements[5] were defined as follows:

"Visible Initiation" - that cavitation condition in which a continuous ring of cavitation is visible at throat discharge.

"Cavitation to Nose" - cavitation terminates at the axial position corresponding to the location of the nose or upstream end of the test specimens (when they are inserted for cavitation damage studies).

"Standard Cavitation" - cavitation terminates at the middle of of the damage specimens.

"Cavitation to Back" - has its termination at the back or downstream end of the test specimen.

"First Mark Cavitation" - has the termination 1-3/4 inches downstream of the throat exit. It may be noted that this is also downstream of the specimens.

B. Derivation of Relation Between Count-Rate and Density

Figure 21 represents the cross-section of the venturi at any particular axial position z. Let R be the venturi radius, t the path length of the radiation within the area, and x the horizontal distance from the venturi center line to the collimator center line. Also let

n_o = number of photons/sec. emitted by the source in such a direction that if they are unscattered, would pass through

the slit of area A of both collimators and strike the detector.

$n_1(x)$ = Photons/sec. passing unscattered through the entire test section, at a distance x, for any cavitation condition.

$n_2(x)$ = Photons/sec. passing unscattered through the entire test section at a distance x, when there is no cavitation.

$\rho(x)$ = Average density of the vertical column of fluid, located at a distance x, and which has a cross section equal to the area A of the collimator slit.

h = Maximum vertical dimension of the test section, as shown in Figure 21.

Then:

$$n_1(x) = n_o \, e^{-\mu_p (h-t)} \, e^{-\beta \rho(x) t} \qquad (1)$$

$$n_2(x) = n_o \, e^{-\mu_p (h-t)} \, e^{-\beta \rho t} \qquad (2)$$

where: ρ = density of mercury = 221.977 gm/in^3

μ = linear absorption coefficient for mercury for 1.17 Mev gamma radiation.

= 2.1 in^{-1}

$\beta = \mu/\rho$ = mass absorption coefficient for 1.17 Mev gamma ratiation.

μ_p = linear absorption coefficient of the Plexiglas for 1.17 Mev gamma radiation.

Dividing (2) by (1) and taking the natural logarithm we get:

$$\ln \frac{n_2(x)}{n_1(x)} = \beta t \left[\rho(x) - \rho\right]$$

$$\rho(x) = \rho + \frac{1}{\beta t} \ln \frac{n_2(x)}{n_1(x)} \qquad (3)$$

In this series of tests $x = 0$, so we have:

$$\rho(0) = \rho + \frac{1}{2R} \ln \frac{n_2(0)}{n_1(0)} \qquad (4)$$

With respect to equation (4) several things may be noted: In a cavitation region, $n_2 < n_1$; so the average density will be less than ρ, the density of liquid mercury. The relation is independent of the collimator opening, provided the source is monoenergetic, and the opening small enough so that the average density may be considered as a constant within the corresponding vertical mercury column. The number of photons per sec., n_1 and n_2, may be replaced by the actual count-rates since detector efficiences cancel in equation (4)

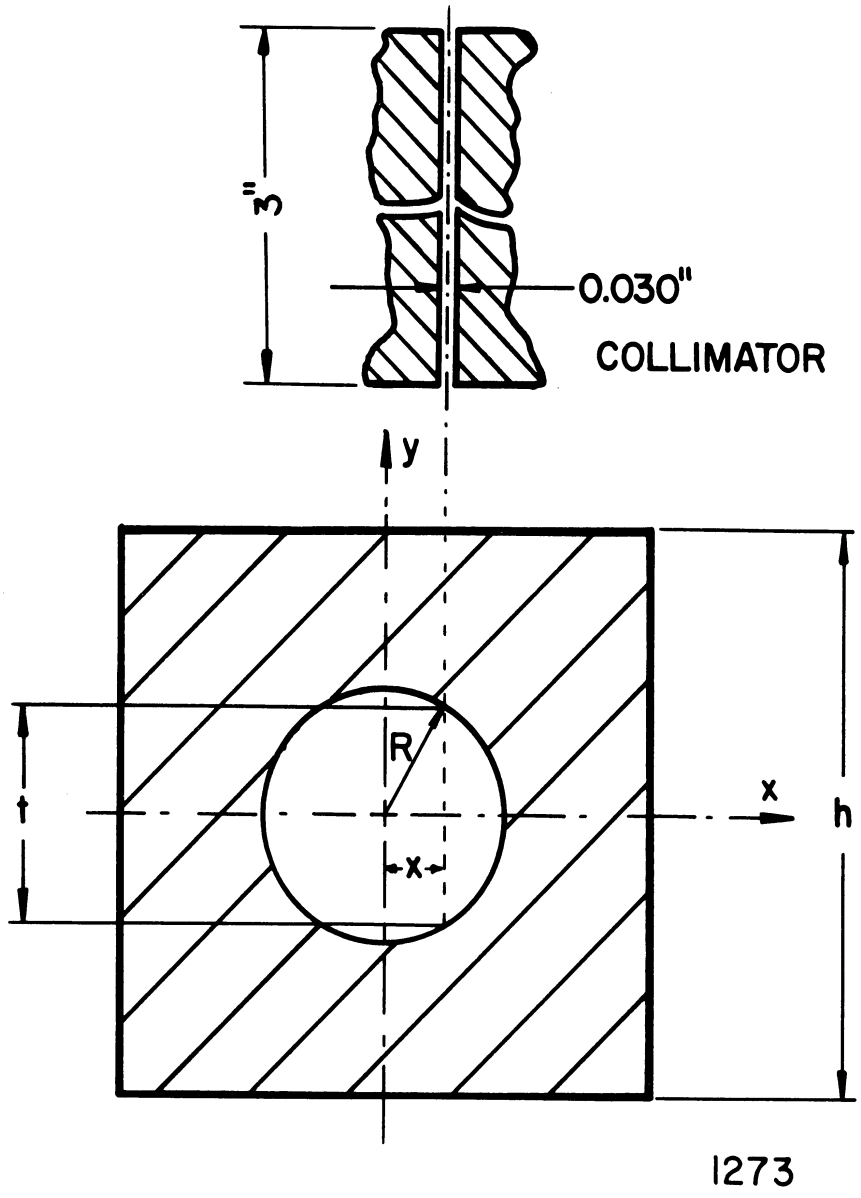

Figure 21. Venturi cross-section as used in density calculations.

C. Central Jet Axial Density Profile Determination

Reference 5 presents void fraction contours for various cavitation conditions as sketched below:

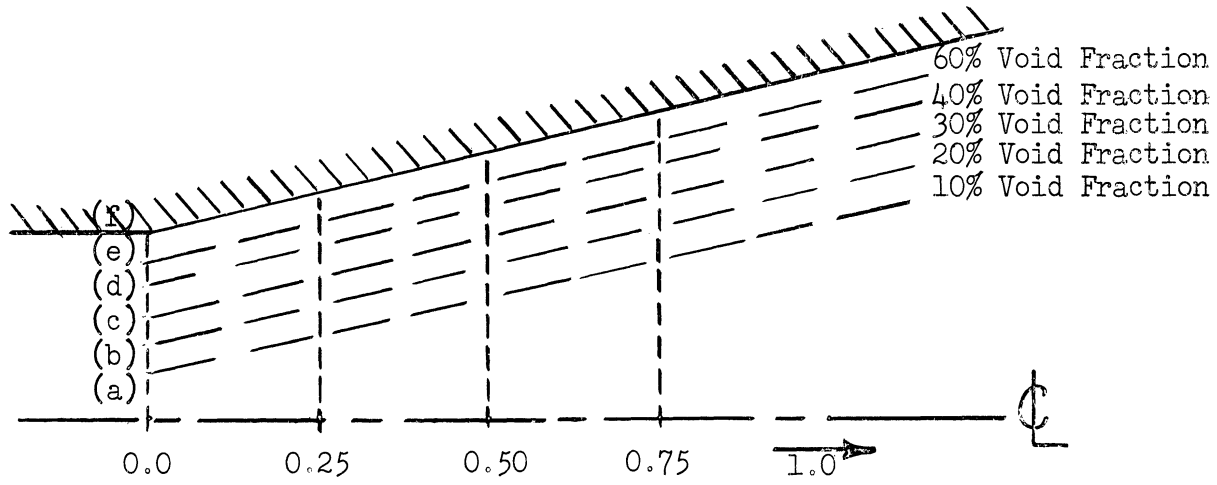

Figure 22. Void fraction contour schematic.

Consider a vertical fluid column of unit cross-sectional area, passing through the center line at any given axial position. Divide this column into segments each extending between adjacent void fraction contours (Figure 22).

Then the total mass in such a fluid column is:

$$\Delta r_{o-a}\,\rho_{o,a} + \Delta r_{a-b}\,\bar{\rho}_{a,b} - - - - - + \Delta r_{e-f}\,\bar{\rho}_{e,f} \qquad (1)$$

$$= \Delta r_{o-a}\,(1 - \overline{V.F.}_{o,a})\,\rho_L + - - - - + \Delta r_{e-f}\,(1 - \overline{V.F.}_{e,f})\,\rho_L \qquad (2)$$

$$= \bar{\rho}\, r_f$$

Thus $$\bar{\rho}/\rho_L = \frac{\Delta r_{o-a}\,(1-\overline{V.F.}_{o-a} - - - + \Delta r_{e-f}\,(1-\overline{V.F.}_{e,f})}{r_f} \qquad (3)$$

In the right-hand side of eq. (3), all quantities are measured[5] except for $\overline{V.F.}_{o-a}$, which is stated to be less than 10%. The left-hand side is known from the data of the present report.

Hence eq. (3) may be solved for $V.F._{o-a}$ and it is these values which are plotted in Figures 15, 16, and 18.

Appendix C Nomenclature:

Δr_{ij} = Radial increment between radius r_i and r_j over which the void fraction changes by about 10%.

$\overline{\rho}_{ij}$ = Average fluid density in the annular ring formed by r_i and r_j, or also the average density in the portion of the vertical column of unit cross section area between r_i and r_j.

$\overline{V.F.}_{ij}$ = Average void fraction in annular ring, between r_i and r_j.

(Detailed calculations are filed under Project 03424, FGH calculations, 9/16/63.)